Boundary element analysis of 3D linear potential problems combining fast multipole expansion and machine-precision numerical integration

Ney Augusto Dumont[1], Hilton Marques Souza Santana[1]

[1]*Department of Civil and Environmental Engineering, Pontifical Catholic University of Rio de Janeiro*
Rua Marquês de São Vicente 225, 22451-900, Rio de Janeiro, Brazil
dumont@puc-rio.br, hiltonmarquess@gmail.com

Abstract. This paper is part of a research work to implement, test, and apply a novel numerical tool that can simulate on a personal computer and in just a few minutes a problem of potential or elasticity with up to tens of millions of degrees of freedom. The authors have already developed their own version of the fast multipole method (FMM) for two-dimensional problems, which relies on a consistent construction of the single-layer potential matrix of the collocation boundary element method (BEM) so that ultimately only polynomial terms (as for the double-layer potential matrix) are required to be integrated along generally curved segments related to a given field expansion pole. The core of the present paper is the mathematical assessment of the double expansions needed in the 3D FMM. The 3D implementation is combined with a particular formulation for linear triangle elements in which all integrations for adjacent source point and boundary element are carried out analytically. As a result, numerical approximations are due exclusively to the FMM series truncations. This allows isolating and testing truncation errors incurred in the series expansions – and thus for the first time properly assessing the mathematical features of the FMM, as illustrated by means of an example. The complete solution of a mixed boundary problem using a GMRES solver, for instance, is just an additional task and, although already implemented, is not reported herein.

Keywords: Fast multipole, Collocation boundary element method, 3D Potential problems, Numerical integration, Analytical integration

1 Introduction

The fast multipole method [1, 2] is a powerful tool for dealing with very large computational mechanics problems. Our team has already developed a consistent algorithm for general 2D problems [3, 4] with machine-precision integration schemes and is now working on 3D problems [5, 6] with the combination of analytical evaluations for flat boundary elements [7, 8]. We develop in this short communication some conceptual aspects that should make the fast multipole method more consistent and understandable mathematically. Although the implementation issues of the complete boundary element formulation are not shown, a simple but thoroughly assessed example shall shed light on the practical application possibilities opened up in the present framework.

2 Problem formulation

We are looking for the expansion of the fundamental solution – for three-dimensional problems – about a pole $\mathbf{x}_c$ that is at the distance $r = |\mathbf{x}|$ from the source point $\mathbf{x}_s$, that is, $\mathbf{x} = \mathbf{x}_s - \mathbf{x}_c$ in the classical literature notation, and to be evaluated at a field point $\mathbf{x}_f$ at a distance $\rho = |\mathbf{y}|$ to the expansion pole, that is, $\mathbf{y} = \mathbf{x}_f - \mathbf{x}_c$ (see the top left drawing in Fig. 1, which gives the vector orientations we are following in the developments):

$$u^*(\mathbf{x}_f - \mathbf{x}_s) \equiv \frac{1}{4\pi\,|\mathbf{x}_f - \mathbf{x}_s|} \approx \frac{1}{4\pi} \sum_{n=0}^{N} \sum_{m=-n}^{n} \bar{S}_{n,m}(\mathbf{x}) R_{n,m}(\mathbf{y}) + O\left(\rho^{N+1}/r^{N+1}\right) \tag{1}$$

up to a given level N of expansion and truncation order $O\left(\rho^{N+1}/r^{N+1}\right)$, which may be immediately inferred from the one-dimensional expansion, for instance: $\frac{1}{x_f-x_s} = \frac{1}{x_c-x_s}\sum_{n=0}^{\infty}\left(-\frac{x_f-x_c}{x_c-x_s}\right)^n$, and as detailed below, where

$$S_{n,m}(\mathbf{x}) = \frac{(n-m)!P_n^m(\cos\theta)e^{im\,\phi}}{r^{n+1}};\; R_{n,m}(\mathbf{y}) = \frac{P_n^m(\cos\beta)e^{im\,\alpha}}{(n+m)!}\rho^n;\; P_n^m(x) = \frac{(1-x^2)^{m/2}}{2^n n!}\frac{d^{n+m}}{dx^{n+m}}(x^2-1)^n. \quad (2)$$

In these equations, $P_n^m(x)$ are associated Legendre functions (polynomials). Both $S_{n,m}(\mathbf{x})$ and $R_{n,m}(\mathbf{x})$ are spherical harmonic functions. As reported by Gumerov and Duraiswami [1], the function name "S" above stands for *source* or *sender* and, coincidentally, also for *singular* (as $r \to 0$), whereas "R" means *receiver* as well as *regular*, which is much appropriate. According to the notation in eq. (1), each level $n = 0, 1, \ldots, N$ comprises $2n+1$ terms. However, $S_{n,-m}(\mathbf{x}) = (-1)^m \bar{S}_{n,m}(\mathbf{x})$ and $R_{n,-m}(\mathbf{y}) = (-1)^m \bar{R}_{n,m}(\mathbf{y})$, $m = 1 \ldots n$. The expressions of $S_{n,m}(\mathbf{x})$ and $R_{n,m}(\mathbf{x})$ are preferably transformed to Cartesian coordinates, that is, $\mathbf{x} = \mathbf{x}_s - \mathbf{x}_c \equiv (x_1, x_2, x_3) \Leftrightarrow (r, \theta, \phi)$ and $\mathbf{y} = \mathbf{x}_f - \mathbf{x}_c \equiv (y_1, y_2, y_3) \Leftrightarrow (\rho, \beta, \alpha)$, such that

$$\mathbf{x} =< r\cos\phi\sin\theta, r\sin\phi\sin\theta, r\cos\theta >, \quad \mathbf{y} =< \rho\cos\alpha\sin\beta, \rho\sin\alpha\sin\beta, \rho\cos\beta > . \quad (3)$$

Moreover, using the complex notation $x = x_1 + x_2 i$, $y = y_1 + y_2 i$ we are able to express $r^{2n+1}\bar{S}_{n,m}(\mathbf{x})$ and $R_{n,m}(\mathbf{y})$ compactly in Cartesian coordinates, as illustrated for $m = 0 \ldots n,\ n = 0 \ldots 4$:

$$r^{2n+1}\bar{S}_{n,m}(\mathbf{x}) \to \begin{array}{ccccc} 1 & . & . & . & . \\ x_3 & \bar{x} & . & . & . \\ -|x|^2 + 2x_3^2 & 3\bar{x}x_3 & 3\bar{x}^2 & . & . \\ -9|x|^2 x_3 + 6x_3^3 & -3\bar{x}\left(|x|^2 - 4x_3^2\right) & 15x_3\bar{x}^2 & 15\bar{x}^3 & . \\ 9|x|^4 - 72x_3^2|x|^2 + 24x_3^4 & -15\bar{x}x_3\left(3|x|^2 - 4x_3^2\right) & -15\bar{x}^2\left(|x|^2 - 6x_3^2\right) & 105x_3\bar{x}^3 & 105\bar{x}^4 \end{array} \quad (4)$$

$$R_{n,m}(\mathbf{y}) \to \begin{array}{ccccc} 1 & . & . & . & . \\ y_3 & \frac{1}{2}y & . & . & . \\ -\frac{1}{4}|y|^2 + \frac{1}{2}y_3^2 & \frac{1}{2}yy_3 & \frac{1}{8}y^2 & . & . \\ -\frac{1}{4}|y|^2 y_3 + \frac{1}{6}y_3^3 & -\frac{1}{16}y\left(|y|^2 - 4y_3^2\right) & \frac{1}{8}y_3y^2 & \frac{1}{48}y^3 & . \\ \frac{1}{64}|y|^4 - \frac{1}{8}y_3^2|y|^2 + \frac{1}{24}y_3^4 & -\frac{1}{48}yy_3\left(3|y|^2 - 4y_3^2\right) & -\frac{1}{96}y^2\left(|y|^2 - 6y_3^2\right) & \frac{1}{48}y_3y^3 & \frac{1}{384}y^4. \end{array} \quad (5)$$

These expressions can be pre-evaluated for a large number N of expansion levels using a symbolic software, such as Maple[1] – and some ingenuity – and stored in arrays. In spite of the complex-variable notation, the indicated sum for every value of n in eq. (1) becomes real. In fact, it has been checked that each expansion level $n = 0 \ldots N$ in eq. (1) corresponds exactly to level $n+1$ of the multivariate Taylor series expansion of $1/4\pi|\mathbf{x}_f - \mathbf{x}_s|$ about $\mathbf{x}_c$, resulting in the truncation error $O\left(\rho^{N+1}/r^{N+1}\right)$, as indicated. We must only pay attention to the orientation of the vector $\mathbf{x}_c - \mathbf{x}_s$, as shown in the left scheme of Fig. 1, which is just a notation subtlety introduced in the technical literature on the subject.

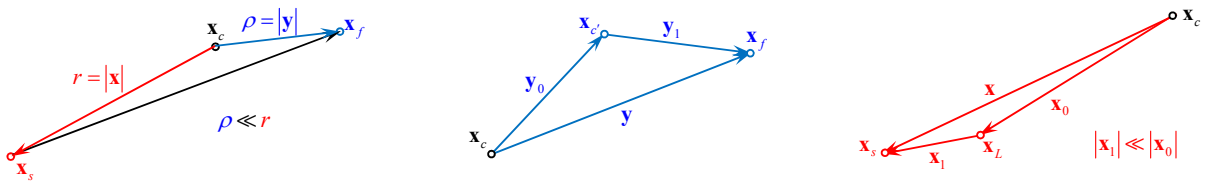

Figure 1. Basic scheme of an expansion about a pole $\mathbf{x}_c$ and schemes for further expansions about a field pole $\mathbf{x}'_c$ and a source pole $\mathbf{x}_L$

[1]Maple 15. Maplesoft, a division of Waterloo Maple Inc., Waterloo, Ontario.

3 Expression of the normal gradient to the boundary

3.1 Expansion using derivatives with respect to the source point

We propose to apply the complex notation for the derivatives of $S_{n,m}(\mathbf{x})$ about the source point, so that just one level more of terms $S_{n+1,m-1}(\mathbf{x})$ needs to be pre-evaluated and stored in the evaluations:

$$\frac{\partial \bar{S}_{n,m}(\mathbf{x})}{\partial x_1} + i\frac{\partial \bar{S}_{n,m}(\mathbf{x})}{\partial x_2} = \bar{S}_{n+1,m-1}(\mathbf{x}), \quad \frac{\partial \bar{S}_{n,m}(\mathbf{x})}{\partial x_3} = -\bar{S}_{n+1,m}(\mathbf{x}). \tag{6}$$

Making use of the notation $\vec{n} =< n_x\ n_y\ n_z >$ as well as of $n = n_x + in_y$ for the components of the normal vector to the boundary, the normal gradient of the potential field to the boundary turns out to be expressed as simply as

$$\begin{aligned} q^* &= -q_x^* n_x - q_y^* n_y - q_z^* n_z = k\frac{\partial u^*(\mathbf{x})}{\partial n} = \frac{k}{4\pi}\left[\frac{\partial u^*(\mathbf{x})}{\partial x_f}n_x + \frac{\partial u^*(\mathbf{x})}{\partial y_f}n_y + \frac{\partial u^*(\mathbf{x})}{\partial z_f}n_z\right] \\ &= \frac{k}{4\pi}\Re\left[\sum_{n=0}^{N}\sum_{m=-n}^{n}\left(-\bar{S}_{n+1,m-1}(\mathbf{x})R_{n,m}(\mathbf{y})\bar{n} + \bar{S}_{n+1,m}(\mathbf{x})R_{n,m}(\mathbf{y})n_z\right)\right]. \end{aligned} \tag{7}$$

3.2 Expansion using derivatives with respect to the field point

Another possibility is to write the derivatives of $R_{n,m}(\mathbf{y})$ about the field point in complex notation

$$\begin{aligned} \frac{\partial R_{n,m}(\mathbf{y})}{\partial y_1} + i\frac{\partial R_{n,m}(\mathbf{y})}{\partial y_2} &= \begin{cases} -R_{n-1,m+1}(\mathbf{y}) & \text{if} \quad -n \le m \le n-2 \\ 0 & \text{otherwise} \end{cases} \\ \frac{\partial R_{n,m}(\mathbf{y})}{\partial y_3} &= \begin{cases} R_{n-1,m}(\mathbf{y}) & \text{if} \quad -n+1 \le m \le n-1 \\ 0 & \text{otherwise,} \end{cases} \end{aligned} \tag{8}$$

which leads, from the expression of the normal gradient to the boundary developed in the first row of eq. (7), to

$$q^* = \frac{k}{4\pi}\Re\sum_{n=1}^{N}\left(\sum_{m=-n}^{n-2}\bar{S}_{n,m}(\mathbf{x})R_{n-1,m+1}(\mathbf{y})\,\bar{n} - \sum_{m=-n+1}^{n-1}\bar{S}_{n,m}(\mathbf{x})R_{n-1,m}(\mathbf{y})\,n_z\right). \tag{9}$$

This equation corresponds to the findings in the technical literature, although the proposed compact format is more convenient for code implementation. It remains to check whether it is correct, which is done in the next Section.

3.3 A numerical comparison

The developments in eq. (7), obtained from

$$\frac{\partial u^*(\mathbf{x}_f - \mathbf{x}_s)}{\partial \mathbf{x}_f} = -\frac{\partial u^*(\mathbf{x}_f - \mathbf{x}_s)}{\partial \mathbf{x}_s} = \frac{k}{4\pi}\sum_{n=0}^{N}\sum_{m=-n}^{n}\frac{\partial \bar{S}_{n,m}(\mathbf{x})}{\partial \mathbf{x}}R_{n,m}(\mathbf{y}) + O\left(\rho^{N+1}/r^{N+1}\right), \tag{10}$$

correspond to expansions in terms of multivariate Taylor series expansions, as checked symbolically with the Maple code. On the other hand, the technical literature shows the results that lead to eq. (9) as

$$\frac{\partial u^*(\mathbf{x}_f - \mathbf{x}_s)}{\partial \mathbf{x}_f} = \frac{k}{4\pi}\sum_{n=0}^{N}\sum_{m=-n}^{n}\bar{S}_{n,m}(\mathbf{x})\frac{\partial R_{n,m}(\mathbf{y})}{\partial \mathbf{y}} + O\left(?\right) \quad \text{for } \rho \ll r, \tag{11}$$

although in general omitting that we are dealing with a truncation. The latter expansion does not correspond to a multivariate Taylor series expansions and one might wonder which approach is more accurate. This is assessed by means of two examples, both for $\mathbf{x}_f =< -11, 30.1, -30.1 >$ and $\mathbf{x}_s = \mathbf{0}$, but different expansion poles, $\mathbf{x}_c =< -11, 30, -30.1 >$ and $\mathbf{x}_c =< -11, 40, -30.1 >$, which leads to the ratios $\rho/r \approx 0.02317$ and $\rho/r \approx 0.19515$. Derivatives $\partial u^*(\mathbf{x}_f - \mathbf{x}_s)/\partial \mathbf{x}_f$ in the Cartesian coordinates are obtained according to eqs. (10) and (11), for $N = 0 \ldots 10$ expansion levels, and Frobenius error norms are plotted as shown on the left in Fig. 2. The solid, black lines are the expected error orders $(\rho/r)^{N+1}$ of a multivariate Taylor series expansion. The longdash, blue lines correspond to eq. (10), and the dashdot, red lines follow from eq. (11). We suggest that the use of eq. (10) should be preferred in a code implementation. However, the better results shown with eq. (10) cannot be proved to be a rule, as we have checked that for a few geometric configurations and values of N eq. (11) performs better.

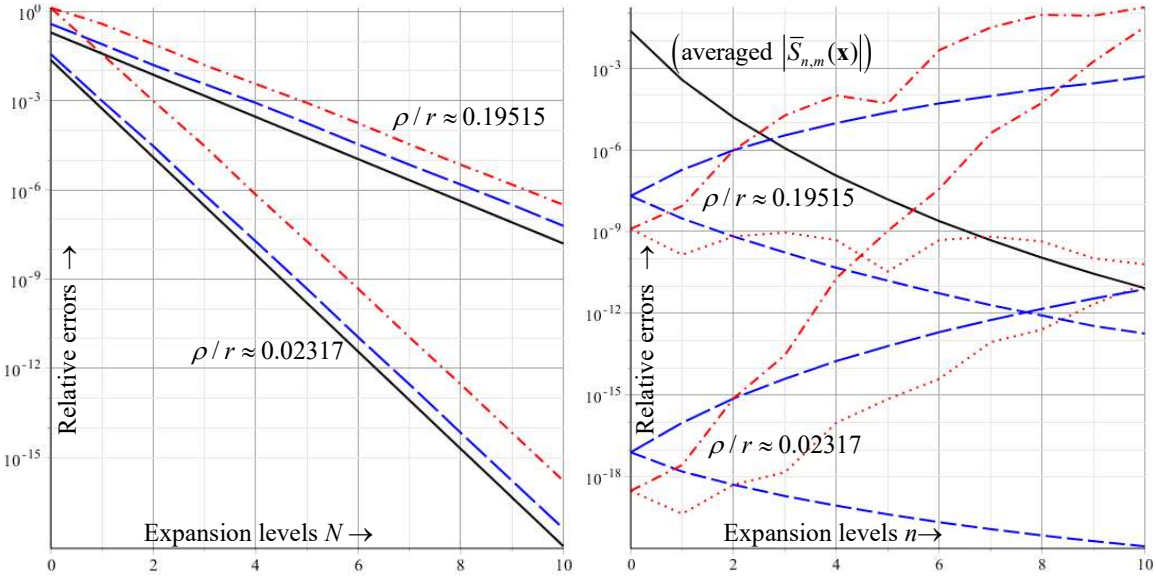

Figure 2. Left: relative errors of eqs. (10) (longdash) and (11) (dashdot), using $(\rho/r)^{N+1}$ (solid lines) as reference, for $N = 0 \ldots 10$; right: error assessments of eq. (13) (dashdot and dot) referred to averaged values of $\left|\bar{S}_{n,m}(\mathbf{x})\right|$, $n = 0 \ldots 10$ (solid), and compared with multivariate Taylor series expansions (longdash and dash lines)

4 Expansion of $R_{n,m}(\mathbf{x}_f - \mathbf{x}_c)$ about a new field pole $\mathbf{x}_{c'}$

The expansion of $R_{n,m}(\mathbf{x}_f - \mathbf{x}_c)$ in any of eqs. (1), (7), (9) for $\mathbf{x}_f$ about a new pole $\mathbf{x}_{c'}$ can be exactly expressed, since $R_{n,m}(\mathbf{x}_f - \mathbf{x}_c)$ are polynomial terms, as

$$\underbrace{R_{n,m}(\mathbf{y})}_{\longleftrightarrow} \equiv \sum_{n'=0}^{n} \sum_{m'=-n'}^{n'} R_{n-n',m-m'}(\mathbf{y}_0) \underbrace{R_{n',m'}(\mathbf{y}_1)}_{\longleftrightarrow} \quad \text{provided that} \quad |m-m'| \leq |n-n'|\,, \tag{12}$$

where $\mathbf{y} \equiv \mathbf{x}_f - \mathbf{x}_c = (\mathbf{x}_f - \mathbf{x}_{c'}) + (\mathbf{x}_{c'} - \mathbf{x}_c) = \mathbf{y}_1 + \mathbf{y}_0$ (see the middle drawing of Fig. 1). Observe that, for successive expansions of the marked term, we characterize a level zero of expansion and follow from there on – expanding $\underbrace{R_{n',m'}(\mathbf{y}_1)}_{\longleftrightarrow}$ for $\mathbf{y}_1 \equiv \mathbf{x}_f - \mathbf{x}_{c'} = (\mathbf{x}_f - \mathbf{x}_{c''}) + (\mathbf{x}_{c''} - \mathbf{x}_{c'}) \equiv \mathbf{y}_1 + \mathbf{y}_0$ as the arguments of a recursive function – until arriving at the highest level. The clause $|m-m'| \leq |n-n'|$ assures the existence condition of $R_{n-n',m-m'}(\mathbf{y}_1)$ – which is void otherwise. We have checked that the above algorithm is equivalent to the multivariate Taylor series expansion of the polynomial terms $R_{n,m}(\mathbf{x}_f - \mathbf{x}_c)$ about $\mathbf{x}_{c'}$. The above equation is not only consistent but also elegant, as the structure of $\underbrace{R_{n,m}(\mathbf{y})}_{\longleftrightarrow}$ is preserved when recursively passed as a function argument. This expression is given in Liu's book [2] [actually very disguised in Eq. (3.55)], although without a reference to the indicated existence condition. This equation is to be applied recursively until we arrive at the highest level of the hierarchical pole development, when we proceed with the required boundary integrations.

5 Expansion of $\bar{S}_{n,m}(\mathbf{x}_s - \mathbf{x}_c)$ about a new source pole $\mathbf{x}_L$

The expansion of $\bar{S}_{n,m}(\mathbf{x}_s - \mathbf{x}_c)$ in any of eqs. (1), (7), (9) for $\mathbf{x}_s$ about a new pole $\mathbf{x}_L$ is [2]

$$\bar{S}_{n,m}(\mathbf{x}) = \sum_{n'=0}^{N} \sum_{m'=-n'}^{n'} \bar{S}_{n+n',m+m'}(\mathbf{x}_0) \underbrace{R_{n',m'}(\mathbf{x}_1)}_{\longleftrightarrow} + O\,(?) \quad \text{for } |\mathbf{x}_1| \ll |\mathbf{x}_0|, \text{ provided that } n+n' \leq N+1, \tag{13}$$

where $\mathbf{x} \equiv \mathbf{x}_s - \mathbf{x}_c = (\mathbf{x}_s - \mathbf{x}_L) + (\mathbf{x}_L - \mathbf{x}_c) = \mathbf{x}_1 + \mathbf{x}_0$ (right drawing of Fig. 1). This expression is not equivalent to a multivariate Taylor series expansion but only a numerical approximation with relative error increasing as n increases.Terms of $\bar{S}_{n,m}(\mathbf{x}_s - \mathbf{x}_c)$ up to level $N+1$ are needed in the expansion, which is consistent with the requirement set after eq. (6). This expression is also given in Liu's book in a very disguised way – a M2L translation, Eq. (3.57), where the multiplication $(-1)^{n'}$ is not applicable when using the argument $(\mathbf{x}_s - \mathbf{x}_c)$ –

and with no reference to the validity condition $n + n' \leq N + 1$ given above. Observe that, if we are interested in further translations of $\underleftrightarrow{R_{n',m'}(\mathbf{x}_1)}$, eq. (12) should be used and then no further approximations take place.

The graph on the right in Fig. 2 gives as reference values averaged $\left|\bar{S}_{n,m}(\mathbf{x})\right| \equiv \sum_{m=-n}^{n} \left|\bar{S}_{n,m}(\mathbf{x})\right|/(2n+1), n = 0 \ldots 10$ plotted as a solid, black line for $\mathbf{x}_s =< -11, 30.1, -30.1 >$ and $\mathbf{x}_c =< 0, 0, 0 >$, and we check that the magnitude of $\bar{S}_{n,m}$ decreases with increasing n (although it is quite invariant with $m = 0 \ldots n$ for a fixed n). We then carry out two numerical assessments, for expansions about $\mathbf{x}_L =< -10, 30, -30 >$ and $\mathbf{x}_L =< -10, 40, -30 >$, in such a way that $|x_1| \,/\, |x_0|$ is either ≈ 0.02317 or ≈ 0.19515. The longdash, blue lines are the relative errors for multivariate Taylor series expansions with error $O(\rho^{N+1}/r^{N+1})$, whereas the dashdot, red lines are relative errors obtained from eq. (13). Although they increase with increasing n, such errors, when related to the largest, averaged values $\left|\bar{S}_{0,m}(\mathbf{x})\right|$, tend to be much smaller, as given by the dash, blue and dot, red lines for multivariate Taylor series and eq. (13), respectively.

6 A simple numerical illustration of a complete FMM implementation

6.1 Problem description

A convex domain in the shape of a tetrahedron as in any of Figs. 3 is initially defined (Level 0) in terms of four faces (triangles) and vertex (node) coordinates, with faces successively subdivided into four triangles each, with the consequent creation of intermediate nodes, according to the following scheme:

$$Coords = \left[\begin{array}{cccc} 1 & 2 & 3 & 4 \\ \hline -3 & 3 & 0 & 0 \\ -1.5 & -1.5 & 1.5 & 0 \\ 0 & 0 & 0 & 4 \end{array}\right]$$

Level	Nodes	Elements	Edges
2	34	64	96
3	130	256	384
4	514	1,024	1,536
5	2,050	4,096	6,144
6	8,194	16,384	24,576
7	32,770	65,536	98,304
8	131,074	262,144	393,216
9	524,290	1,048,576	1,572,864

A succession of analyses is carried out for the implemented fast multipole algorithm with the adjacency criterion Nc = 1, 2 or 3 and using N = 2, 4, 6, 8 or 10 Taylor expansion levels, according to eq. (1). The schemes in Fig. 3 illustrate the case after three subdivisions, which corresponds to level 3 in the Table. This figure also illustrates, for the green-colored triangle at the bottom face and adjacent to the frontal corner, that we first consider, on the left, that only the elements that share a vertex are close to it (Nc = 1), whereas in the middle figure elements are considered close when their parents are adjacent (Nc = 2). The right figure shows the case for adjacency of their parents' parents (Nc = 3). The fast multipole scheme is applied only for elements sufficiently far, that is, the gray-colored elements in the figure as referred to the green-colored element.

6.2 Numerical assessments

Accuracy of the implemented fast multipole scheme is firstly assessed for a linear potential field $u = x+y+z$ applied to the boundary of this tetrahedron, with nodal potentials **d** and gradient parameters **t** evaluated for different mesh refinements, as shown in the Table above. We initially carry out a control analysis in terms of the plain, conventional boundary element method (CBEM) with all integrals evaluated analytically [7, 8], for which the basic equation $\mathbf{Hd} = \mathbf{Gt}$ should be exactly satisfied within machine precision. Since the code is implemented in C++ with double precision, a relative error $\mathbf{e} = \|\mathbf{Hd} - \mathbf{Gt}\| \,/\, \|\mathbf{Hd}\| > 10^{-15}$ is expected to occur and actually increasing round-off errors take place as the number of degrees of freedom increases. This is observed in the graph on the left in Fig. 4 for the error results marked as • related to refinement levels 2 through 6 of the Table. These errors are our achievable, threshold accuracy we can expect in the numerical simulations to come.

Observe that the implementations must start with refinement levels $Nc + 1$ in the Table of Section 6.1. Since the T3 element exactly reproduces a linear potential field and all integrations are carried out within machine precision, the reported errors are due solely to the expansion truncations of the fast multipole scheme, which are related to the truncation order at a given level N and and ultimately depend on Nc. Moreover, round-off

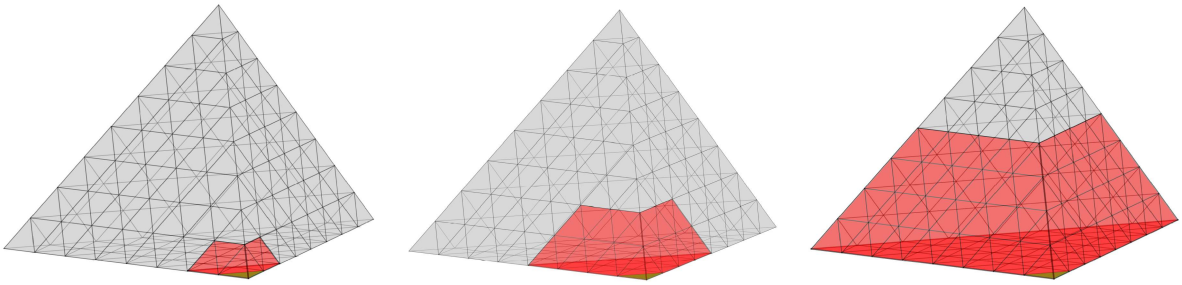

Figure 3. Red-colored elements illustrated as close to the green-colored element on the bottom depending on how restrictive we are in a hierarchical sequence with Nc = 1, 2 or 3

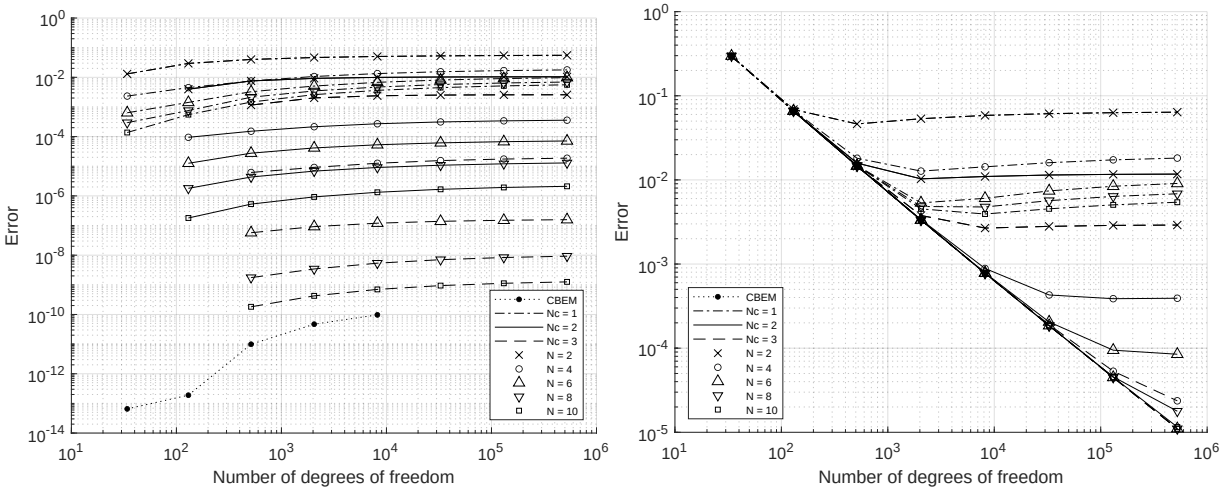

Figure 4. FMM relative error results for applied potential fields $u = x + y + z$ (left) and $u = xyz$ (right)

errors unavoidably occur with increasing node numbers, which is reflected by the ascending curves. These results lead to the accuracy threshold of results achievable in an analysis for the considered domain submitted to a more complicated potential field. In fact, a similar series of analyses carried out for an applied cubic field $u = xyz$, with results displayed on the right in Fig. 4, shows that accuracy convergence follows the pattern of the CBEM implementation until the threshold of the left graph is arrived at. Observe by comparing both graphs that results would still improve if a more refined mesh had been considered for higher values of Nc and N.

Figure 5 shows on the left the computational time required for the matrix-vector multiplications **Hd** and **Gt** of the previous analyses. The computational times are proportional to N^2 and N for the CBEM and the fast multipole operations, respectively, with time shifts perfectly acceptable for higher values of Nc and N, which attests to the advantage of working in such a computational framework even if just a few hundreds of degrees of freedom are required in a simulation. The storage allocation is also relatively small and increases proportionally to the number of degrees of freedom in a loglog plot. The ultimate assessment of the proposed implementation is given in the graph on the right in Fig. 5, as we plot for the applied cubic potential field the relative errors of the right graph in Fig. 4 against the computational time on the left in Fig. 5 for a few values of Nc and N, also comparing with the CBEM. We see that not only the required computational time using the FMM is much smaller for a required error tolerance but also that the performance in terms of convergence rate is by far superior.

7 Conclusions

This short communication focused on the conceptual aspects and the convergence issues of the series expansions needed in the 3D fast multipole developments for potential problems in a way that is not found in the technical literature. Important implementation details – particularly with respect to the recursive application of eqs. (12) and (13) – had to be left to a posterior publication [6] as well as the not lesser aspects of the iterative solution of a practical problem. A very simple example, for which all integrals could be evaluated within machine precision, makes evident how important it is to have evaluation precision, computational effort and accuracy of results completely under control.

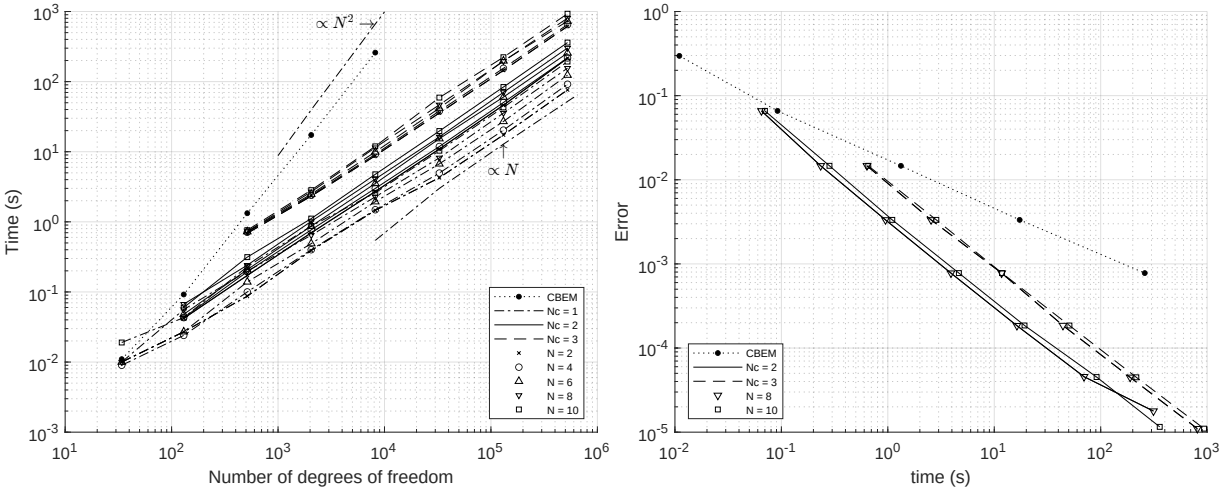

Figure 5. Computational time required for different types of analysis (left) and efficiency assessment of some simulations in terms of error versus time

Acknowledgements. This project was supported by the Brazilian agencies CAPES and CNPq.

Authorship statement. The authors hereby confirm that they are the sole liable persons responsible for the authorship of this work, and that all material of the present paper is the property (and authorship) of the authors.

References

[1] N. A. Gumerov and R. Duraiswami. *Fast Multipole Methods for the Helmholtz Equation in Three Dimensions*. Elsevier, 2004.

[2] Y. Liu. *Fast Multipole Boundary Element Method - Theory and Applications in Engineering*. Cambridge, 2009.

[3] N. A. Dumont and H. F. C. Peixoto. A fast-multipole unified technique for the analysis of potential problems with the boundary element methods. *Proc Indian Natn Sci Acad*, vol. 82, n. 2, pp. 289–299, 2016.

[4] H. F. C. Peixoto. *A Fast Multipole Method for High Order Boundary Elements*. PhD thesis, Pontifícia Universidade Católica do Rio de Janeiro, 2018.

[5] A. R. Florez Ttito. *Implementation of a Fast Multipole Technique for the Solution of Three Dimensional Potential and Elasticity Problems*. PhD thesis, Pontifícia Universidade Católica do Rio de Janeiro. (In Portuguese), 2020.

[6] H. M. S. Santana. Implementation of a consistent fast multipole technique for the solution of threedimensional potential problems. Master's thesis, Pontifícia Universidade Católica de Rio de Janeiro. (In progress), 2021.

[7] N. A. Dumont and T. G. Kurz. Analytical 3D boundary element implementation of flat triangle and quadrilateral elements for potential and linear elasticity problems. In A. H.-D. Cheng and A. Tadeu, eds, *Boundary Elements and other Mesh Reduction Methods XLII*, volume 26 of *WIT Transactions on Engineering Sciences*, pp. 1–11. WIT Press, 2019.

[8] T. G. Kurz. *Analytical evaluation of the integrals of flat boundary elements for three-dimensional potential and elasticity problems*. PhD thesis, Pontifícia Universidade Católica do Rio de Janeiro. (In Portuguese), 2021.